Technical Report Documentation Page

1. Report No.	2. Government Accession No.	3. Recipient's Catalog No.
Pending assignment.	N/A	N/A

4. Title and Subtitle	5. Report Date
Enhanced Cybersecurity via Smart Antenna Technology for V2X	September 30, 2024
	6. Performing Organization Code N/A

7. Author(s)	8. Performing Organization Report No.
Chi-Chih Chen, Ph.D. https://orcid.org/0000-0001-6016-7708 Julia Wu	N/A

9. Performing Organization Name and Address	10. Work Unit No. (TRAIS)
The Ohio State University Address: 281 W Lane Ave, Columbus, OH 43210	N/A
	11. Contract or Grant No. 69A3552348327

12. Sponsoring Agency Name and Address	13. Type of Report and Period Covered
The Ohio State University Address: 281 W Lane Ave, Columbus, OH 43210	Final (June 2023 to Aug. 2024)
	14. Sponsoring Agency Code N/A

15. Supplementary Notes

Conducted in cooperation with the U.S. Department of Transportation, Federal Highway Administration.

16. Abstract

This project is under the thrust area of "Develop Cyber-resilient Mitigation Methods". The main purpose of this project is developing a smart antenna system to enhance cybersecurity of vehicle-to-everything (V2X) and Cellular V2X (C-V2X) communication in 5.9 GHz frequency band. Our compact and low-cost antenna system comprises a circular array of four antenna elements with specially designed patterns which support both multiple inputs multiple outputs (MIMO) and array beamforming operations. It is also capable for rejecting strong interference or jamming signals due to its specially designed antenna element patterns. Our approach is superior to conventional pure MIMO antenna or phased array antenna design approaches, and thus enhancing V2X communication reliability and security. A protype of the developed antenna system design was fabricated and measured. The measurement results were compared with performance predicted from numerical model simulations with excellent agreement. The developed V2X/C-V2X antenna systems can be used with any existing V2X/C-V2X radios for communication or navigations with enhanced security against multi-path or malicious interferences.

17. Key Words	18. Distribution Statement
vehicle to infrastructure communications, vehicle to vehicle communications, antennas electromagnetic interference, phased array, multipath interference, jamming, multiple inputs multiple outputs (MIMO)	No restrictions. This document is available to the public through NTIS: National Technical Information Service Springfield, Virginia 22161

19. Security Classif.(of this report)	20. Security Classif.(of this page)	21. No. of Pages	22. Price
Unclassified	Unclassified	20 pages	

Form DOT F 1700.7 (8-72) **Reproduction of completed page authorized**

CARMEN+ UTC

Center for Automated Vehicle Research with Multimodal AssurEd Navigation

University Transportation Centers Program

Final Report: Enhanced Cybersecurity via Smart Antenna Technology for V2X

P.I.	Project Info:
Chi-Chih Chen, Ph.D. Research Associate Professor The Ohio State University Electrical and Computer Engineering Department	Grant No. 69A3552348327 DUNS: 832127323 EIN #: 31-6025986 Project Effective: June 1, 2023 Project End: August 30, 2024 Submission: September 30, 2024

Consortium Members:

THE OHIO STATE UNIVERSITY
COLLEGE OF ENGINEERING

UCI University of California, Irvine

TEXAS The University of Texas at Austin

NORTH CAROLINA AGRICULTURAL AND TECHNICAL STATE UNIVERSITY

DISCLAIMER

The contents of this report reflect the views of the authors, who are responsible for the facts and accuracy of the information presented herein. This document is disseminated in the interest of information exchange. The report is funded, partially or entirely, under grant number 69A3552348327 from the U.S. Department of Transportation's University Transportation Centers Program. The U.S. Government assumes no liability for the contents or use thereof.

Table of Contents

1 *Research* Objectives

This research focuses on developing a compact and cost-effective multi-element antenna system for V2X/C-V2X communication, which is crucial for Intelligent Transportation Systems (ITS) and connected autonomous vehicles [1]. V2X/C-V2X faces challenges such as signal blockage, interference, and multi-path signal. While information encryption and advanced coding can address some of these issues, problems like signal blockage and malicious interference need solutions at the antenna stage before reaching the low-noise amplifier and the subsequent digitization stage, thus posing threat to the security of V2X/C-V2X communications [2].

Similar threats have been faced in GPS/GNSS operations and have been mitigated using advanced a combination of multi-element antennas along with simultaneous signal beamforming and interference nulling [3]. However, such technology has not been adapted for V2X/C-V2X due to lack of proper antennas and concerns about cost, size, and weight. This research aims to create a new compact low-cost 4-element antenna system design that balances performance, size, and affordability, enhancing beamforming and interference-nulling capabilities for V2X/C-V2X systems. This approach differs from traditional MIMO methods [4] and promises significant improvements in signal-to-interference-and-noise ratio at the RF front-end. The proposed antenna element design also differs from traditional phased array where each antenna element has broad patterns and is subject to be affected by strong malicious interference.

2 Technical Approaches

The intended RF performance requirements for the 4-channel antenna at each frequency band are listed in Table 1 which includes the frequency ranges, the antenna gain pattern percent coverage, and the envelope correlation coefficient (ECC) [5] for MIMO antenna systems. The antenna pattern percent coverage is the percentage of the antenna gain that meets or exceeds a value of X dBi in a azimuth pattern cut at a given elevation angle, as illustrated in Figure 1, where the coverage region is $-90° \leq \theta \leq 90°$ and $0° \leq \varphi \leq 360°$.

Table 1 Antenna Gain and ECC requirements of common communication systems.

Frequency Range (MHz)	**Frequency Category**	**Antenna Pattern Percent Coverage 90% of Gain ≥ X (dBi)**	**ECC** $ECC = \lvert\rho_c\rvert^2$
617 - 960	5G sub 6	≥ -7	≤ 0.2
1710 - 2200	4G LTE	≥ -5	≤ 0.15
2350 – 2360	4G LTE	≥ -5	≤ 0.15
2401 - 2483	WLAN	≥ -5	≤ 0.15
2500 - 2690	4G LTE	≥ -5	≤ 0.15
3300 - 4200	5G sub 6	≥ -5	≤ 0.15
4400 - 5000	5G sub 6	≥ -5	≤ 0.15
5150 - 5895	WLAN	≥ -5	≤ 0.15
5850 - 5925	C-V2X	≥ -5	≤ 0.15

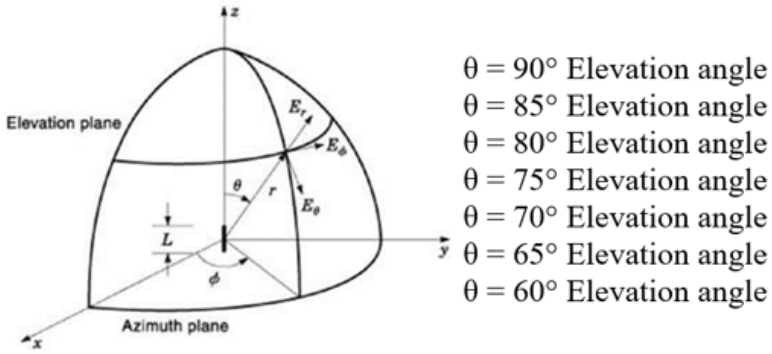

Figure 1: Spherical coordinate system for antenna analysis.

The envelope correlation coefficient (ECC) between two antenna channels, say channel 1 and channel 2, is calculated using Equation (1), where E_1 and E_2 are the complex electrical field radiated by antenna element 1 & 2, respectively; P is the probability distribution of the incident angular power density which is assumed to have a uniform calibration; X is the cross-polarization coupling factor and is assumed to be infinity here. To calculate the ECC, the far-field antenna pattern data is taken for each polarization in complex format and the integral region is $0° \leq \theta \leq 90°$ & $0° \leq \varphi \leq 360°$. Then the formula is applied for ρ_c, and $ECC = |\rho_c|^2$.

$$\rho_c = \frac{\int_\Omega \left(\frac{X}{1+X} E_{1\theta} E_{2\theta}^* P_\theta + \frac{1}{1+X} E_{1\varphi} E_{2\varphi}^* P_\varphi\right) d\Omega}{\left(\sqrt{\int_\Omega \left(\frac{X}{1+X} E_{1\theta} E_{1\theta}^* P_\theta + \frac{1}{1+X} E_{1\varphi} E_{1\varphi}^* P_\varphi\right) d\Omega \times} \sqrt{\int_\Omega \left(\frac{X}{1+X} E_{2\theta} E_{2\theta}^* P_\theta + \frac{1}{1+X} E_{2\varphi} E_{2\varphi}^* P_\varphi\right) d\Omega}\right)} \quad (1)$$

Although traditional MIMO antenna systems with pattern diversities (see Figure 2) can increase channel capacity and reduce multi-path effects, and avoid strong interferences, it does not take the full advantage of the larger antenna aperture to produce higher antenna gain and narrower beamwidth. A higher gain produces stronger signal strength which leads to longer communication range and higher channel capacity. A narrower beamwidth can reduce the probability of interception and interference, which leads to improved communication security.

On the other hand, the beamforming array approach can maximize antenna gain and minimize beam width by combining signals from all antenna elements. However, the major shortcoming of this approach is its lack of protection from strong malicious interference which could disable all elements simultaneously due to broad element patterns.

Therefore, we propose an innovative pattern design approach which allows us to utilize three of the four antenna elements to perform beamforming while each element has an azimuthal pattern blind region (i.e. low gain region), as illustrated in the top row of Figure 2, to protect it from a strong interference source.

Figure 3 depicts the elevation pattern of the proposed antenna design for best supporting V2X/C-V2X applications which emphasize on lower elevation angles.

Figure 2 Different smart antenna system azimuthal pattern design approaches. (Top) proposed design (Middle) Beamforming Array Approach (Bottom) Pattern Diversity MIMO Approach

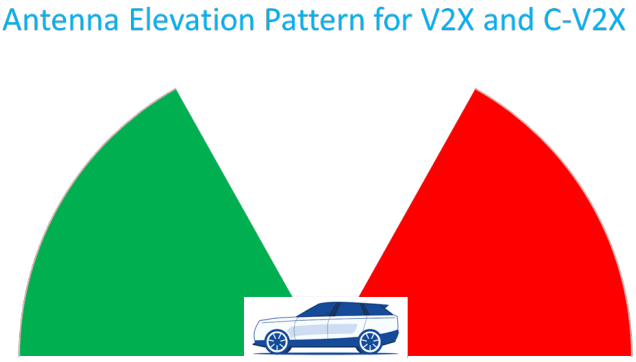

Figure 3 Desired elevation pattern design for V2X/C-V2X applications.

3 Enhanced V2X/C-V2X Antenna System Design

3.1 Array Element Design

3.1.1 Cavity-Backed Monopole Element

We aim to design an antenna operating at 5.9 GHz, with the requirement that the azimuth pattern exhibits a null between -120 degrees and 120 degrees to block strong interference signals. The array element design will be based on a monopole antenna (the yellow strip in Figure 4), which is chosen for its simplicity and easy fabrication. This design approach allows for effective signal reception while meeting the specific interference rejection requirements, making it suitable for the intended application.

This design utilizes a vertical reflecting wall (see Figure 4) behind each monopole element for shaping the azimuth patterns using full-wave electromagnetic numerical model simulations. The wall's width, height, and the distance between the wall and the monopole, were optimized to produce the designed azimuth pattern.

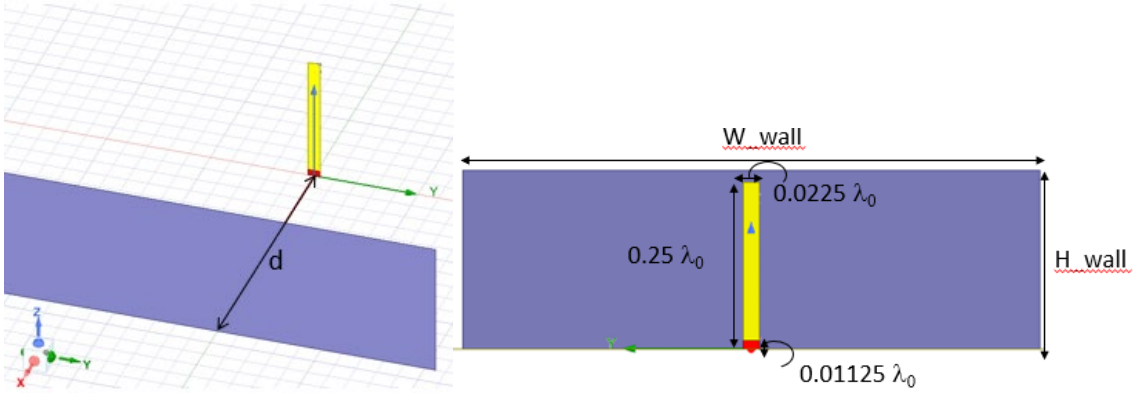

Figure 4: Wall configuration of the new design.

Figure 5 demonstrates the impact of varying wall reflector widths on the antenna's radiation pattern. It is clear that while there is no significant effect on the vertical radiation pattern, the azimuth radiation pattern is noticeably influenced by the width. This suggests that the width of the wall can be used as a control parameter for shaping the azimuth radiation patterns. Moreover, as shown in Figure 6, we analyzed different distances between the wall and the antenna, concluding that the wall-to-antenna distance affects the entire radiation pattern. Finally, Figure 7 reveals that the height of the wall has a direct effect on the vertical radiation pattern, confirming that wall dimensions play a critical role in optimizing the antenna's performance. These observations guide the structural design choices in ensuring effective beam steering and pattern control.

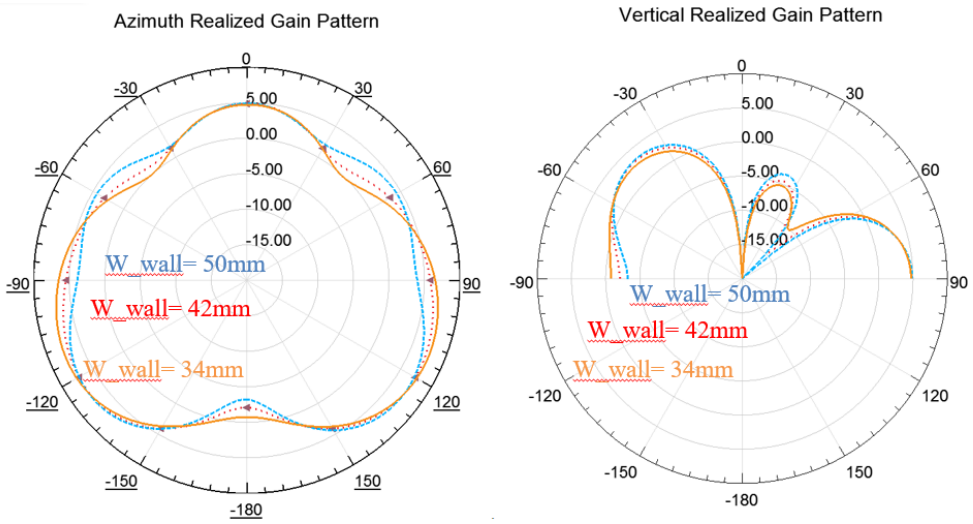

Figure 5：Study of different widths of wall.

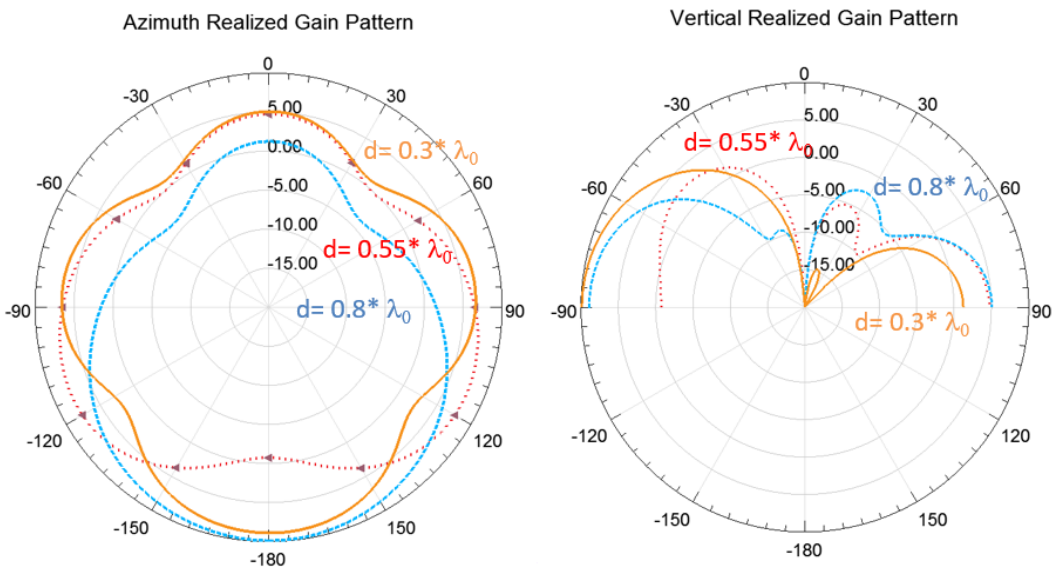

Figure 6: Study of different Distances between Wall and the Antenna.

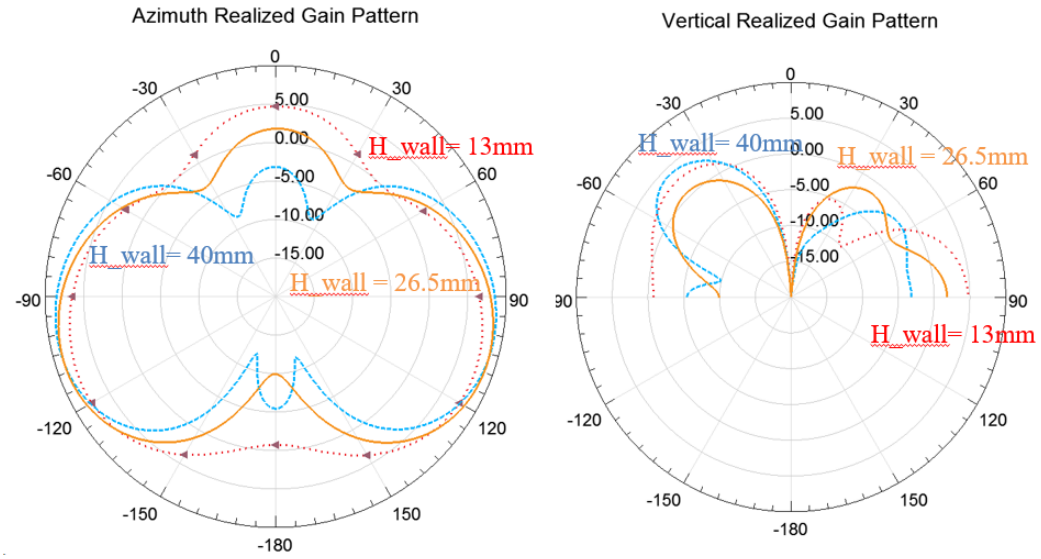

Figure 7: Study of different heights of wall.

3.1.2 Curved-Wall Reflector for Horizontal Pattern Control

A curved-wall reflector is used in antenna design to be more effective in reducing the diffractions from the vertical edges for producing deeper pattern null of the horizontal radiation pattern behind the wall, as demonstrated in Figure 8. By shaping the reflector into a curved configuration, it helps in shaping the azimuth pattern and reducing unwanted side and back lobes. More specifically, this curved design ensures that the antenna can achieve better pattern uniformity over the coverage region and deepening the pattern null in the back direction which is important for strong interference rejection.

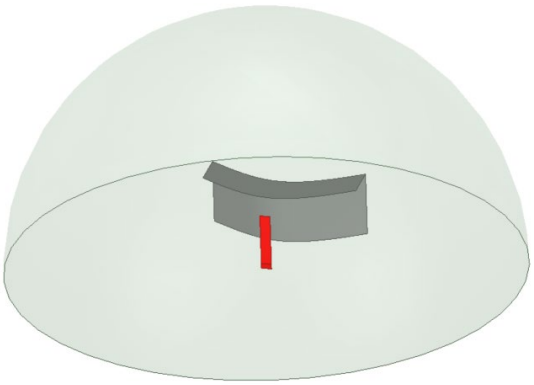

Figure 8 Initial curved reflecting wall design.

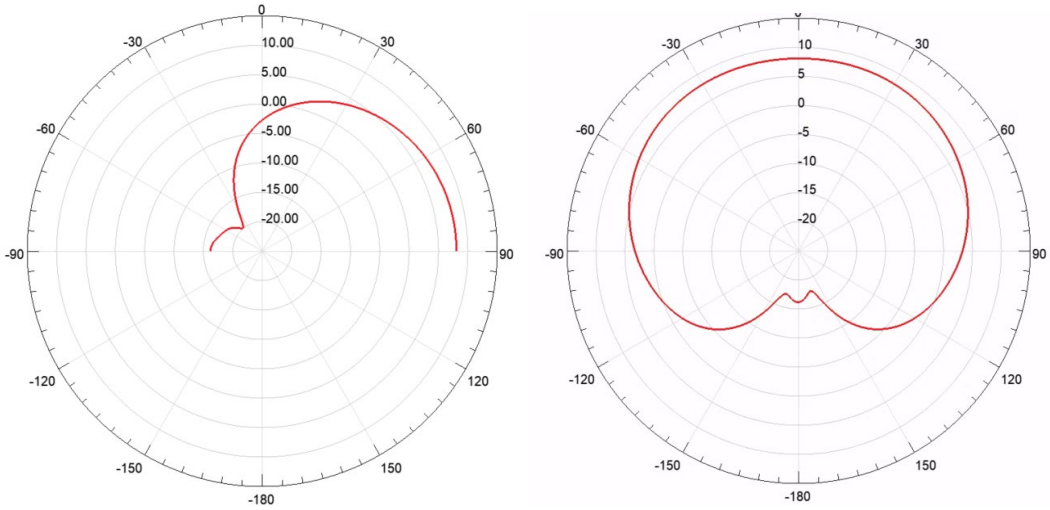

Figure 9 Azimuth (left) and vertical (right) radiation pattern of the curved wall design at 5.9 GHz.

3.1.3 Overhang Deign for Vertical Pattern Control

Adding an overhang on top of the curved reflecting wall (Figure 8) helps shaping the vertical radiation pattern. The roof would act as an additional top reflector, leading to stronger reflections in the vertical plane and producing less diffraction from the top of the wall. The constructive and destructive interferences among the top and side diffractions determine the antenna pattern behind the wall. Additionally, radiation at higher elevation angles could be suppressed, reducing signal strength in those directions. The width of the overhang and its distance to the monopole was carefully optimized to achieve the desired elevation patterns without affecting the resonance of the monopole antenna. Figure 10 shows the elevation and azimuth patterns for different overhang width control parameter, pL_roof. It demonstrates that the overhang roof has a significant effect on the vertical radiation patterns. Among these cases, the pL_roof=0.1 produces lowest backlobe for maximum interference/jamming protection. Further study shows that pL_roof=0.15 produced best pattern performance with minimum backlobe. This corresponds to approximately the overhang width of 7.6mm.

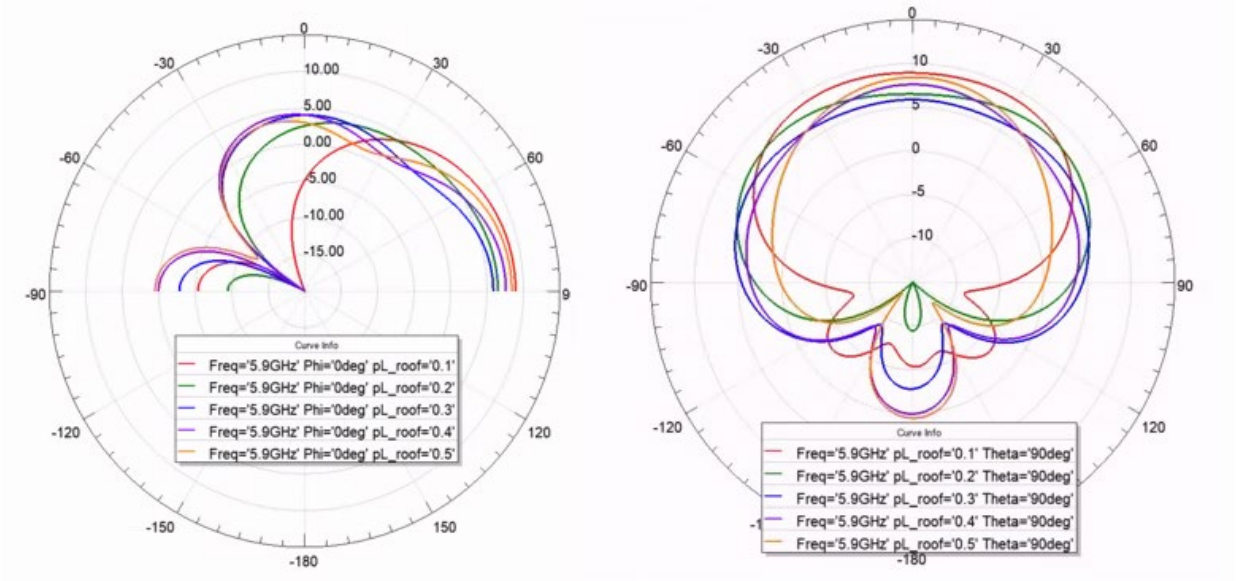

Figure 10 Elevation (left) and azimuth (right) patterns for different overhand width control value.

3.2 4-Elemnt Array Design Optimization

3.2.1 Dimension Study of 4-Element Array

To achieve higher array gain, we plan to position four antennas in a circular configuration, as shown in Figure 11. This arrangement will allow the antennas to work separately in the MIMO mode based on its pattern diversity or together in phased array mode based on its spatial diversity for narrower beam widths and higher. The circular placement ensures that the antennas can cover a broader area while maintaining uniform performance across all azimuth directions. By adjusting the spacing between the antennas and optimizing their phase alignment, we can improve directivity and reduce interference from unwanted angles, ultimately enhancing the array's efficiency and performance in both transmitting and receiving signals. This setup is ideal for applications requiring stronger signal strength and better coverage.

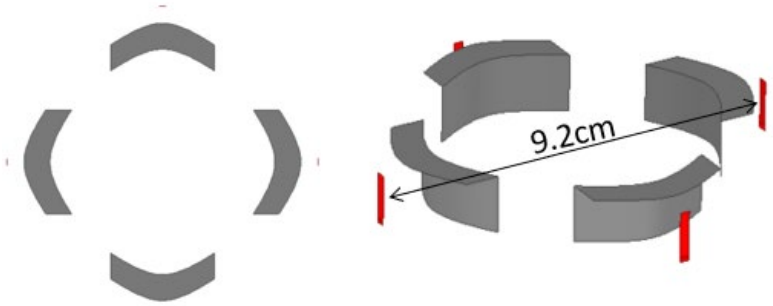

Figure 11: Configuration of four Antennas with Inverted L-Shaped Reflectors.

Figure 12 shows simulated element radiation patterns in the vertical (left) and horizontal (right) plane at 5.9 GHz of 4-element array on an infinite ground plane. These patterns were obtained with only one of the four elements activated while the rest of the array terminated. Figure 13 shows simulated 3D gain pattern plots of each array element.

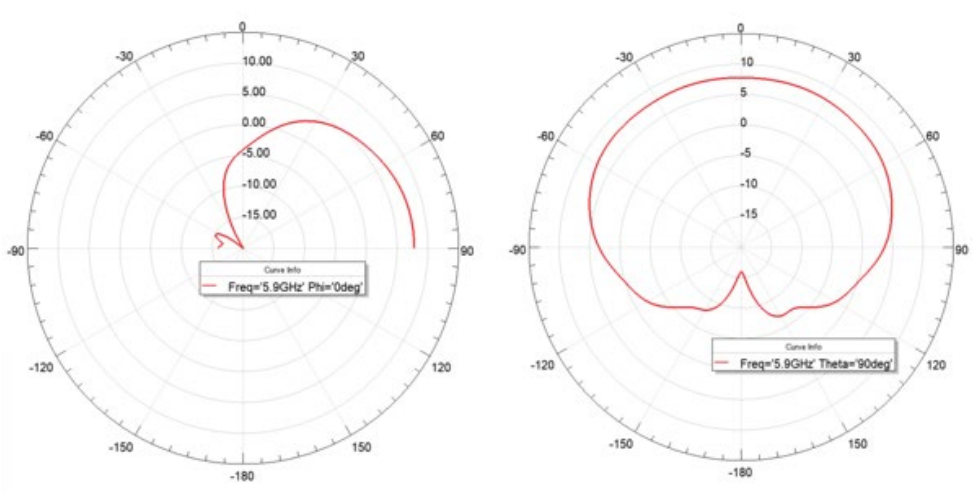

Figure 12: Simulated element radiation patterns in the vertical (left) and horizontal (right) plane at 5.9 GHz of 4-element array on an infinite ground plane.

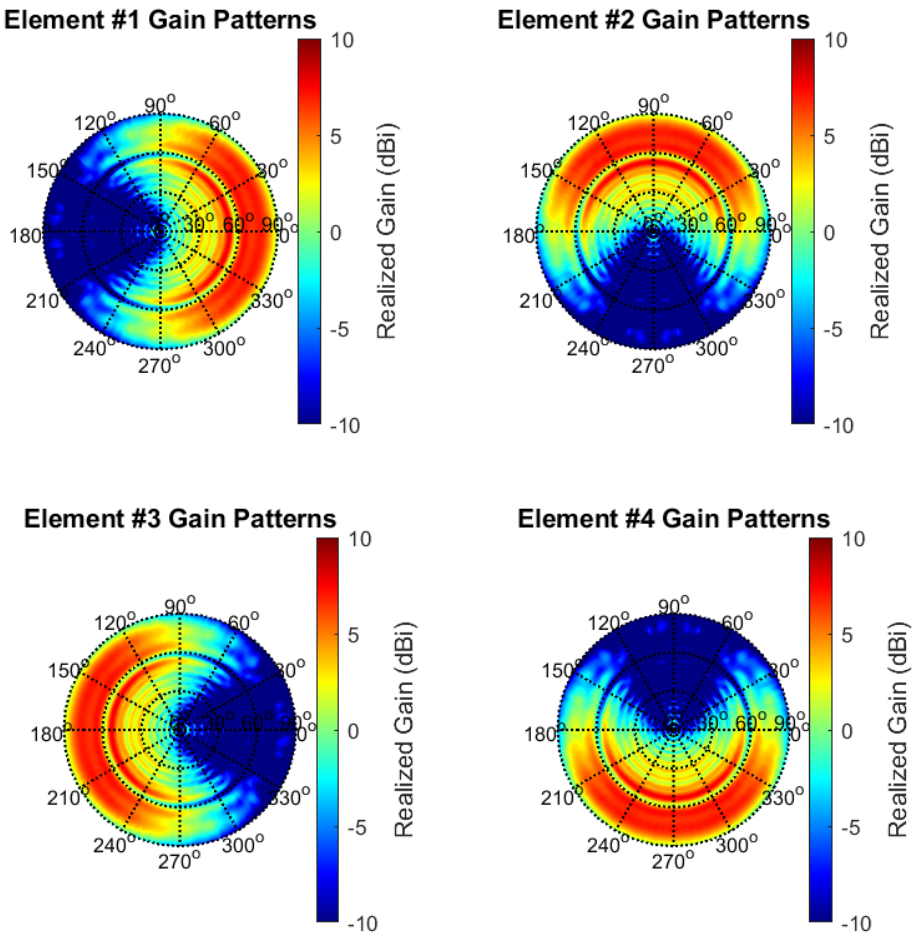

Figure 13 Simulated 3D gain pattern plots of each array element.

Figure 14 illustrates the configuration of the array diameter to be investigated here. Figure 15 presents the S-parameters analysis for different array diameters. From the data, it is evident that even at the smallest gap of 68 mm where the adjacent reflecting walls are touching each other, the mutual coupling parameters S_{12}, S_{13}, S_{14} remain below -20 dB.

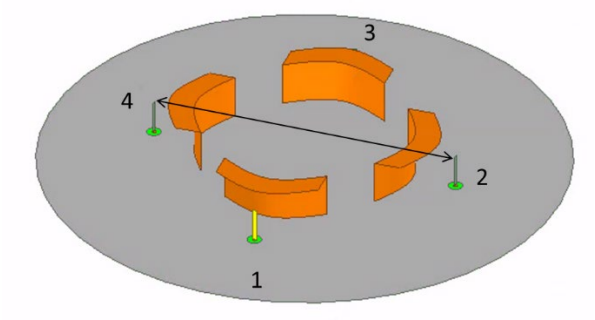

Figure 14 Array dimension (diameter).

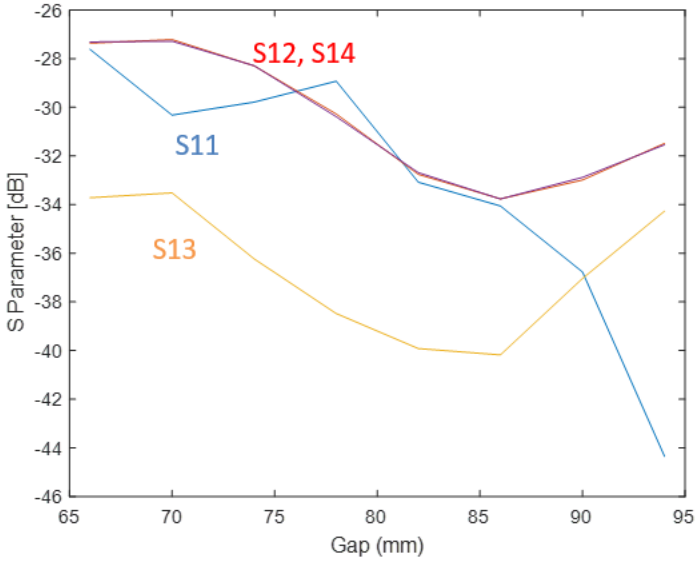

Figure 15 S -Parameters with different array diameters from 68mm to 94mm.

Further analysis in Figure 16 shows the effect of the array diameter on the azimuth and vertical radiation patterns. Specifically, as the diameter increases beyond 90 mm, a null begins to appear in the back lobe of the radiation pattern, which improves interference rejection capability. Although a larger array dimension produces desirable lower back lobe level, it will produce too many grating lobes in phased array mode since the wavelength at 5.9 GHz is approximately 51 mm. We selected an array diameter of 90 mm for the final design, as it provides the best balance between S-parameter performance and desired radiation characteristics.

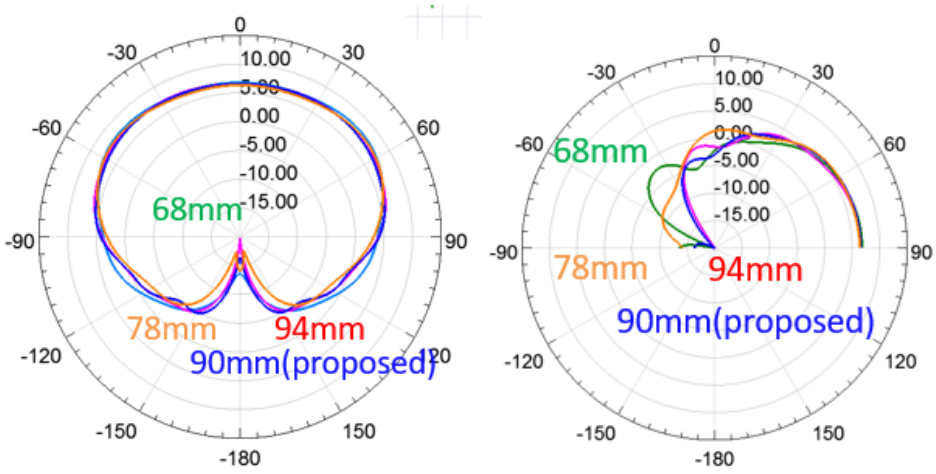

Figure 16 Azimuth(left) and vertical(right) radiation patterns with different array diameters.

3.2.2 Supporting Structure Design

We selected ABS (Acrylonitrile Butadiene Styrene) as the material for 3D printing the antenna due to its favorable properties for antenna fabrication. ABS is known for being a low-loss material in high-frequency applications, which helps minimize signal attenuation and ensures better performance. Its mechanical strength and durability make it suitable for maintaining the structural integrity of the antenna during use. We opted for a material thickness of 1mm to prevent interference with the antenna's electrical performance, ensuring that the material does not significantly impact the resonant frequency or radiation pattern.

Additionally, since our design involves four separate antenna elements, we created a combined structure to assemble these elements into an array to enhance their position accuracy and mechanical stability. To mount the antennas to the aluminum ground plane, we incorporated holes for four nylon screws, allowing for easy assembly and stability of the antenna system. Nylon screws were chosen to avoid any electromagnetic interference, ensuring that the metal components of the assembly do not degrade the antenna's performance. This design approach allows for precise positioning and alignment of the antennas, contributing to better array performance and ease of maintenance. Figure 17 shows the final 4-element V2X/C-V2X array design with antenna elements, ABS supporting structure and the Nylon mounting screws.

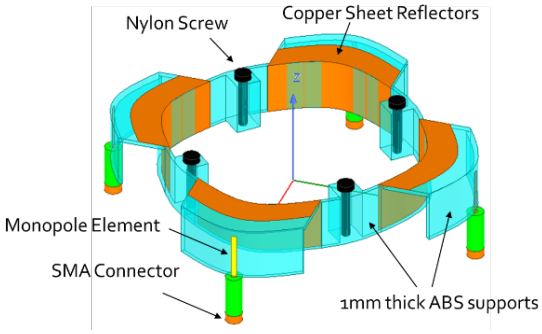

Figure 17: Simulation model configuration.

Figure 18presents the S-parameters of the antenna. From the data, we can observe that the reflection S_{11} is below -10 dB, indicating good impedance matching at the target frequency of 5.9 GHz. This confirms that the antenna is well-tuned to operate at the desired frequency. The antenna mutual couplings S_{12}, S_{13}, and S_{14} are all below -30 dB, indicating excellent isolation between different antenna elements. As expected, S_{13} is lower than both S_{12} and S_{14} This is expected since elements 1 and 3 are positioned at the opposite side of the array with a greater distance between them, which reduces mutual coupling and improves isolation compared to the mutual coupling between adjacent elements. As will be shown later, weaker mutual coupling will lead to higher diversity gain and channel capacity when the array is operated in the MIMO modes.

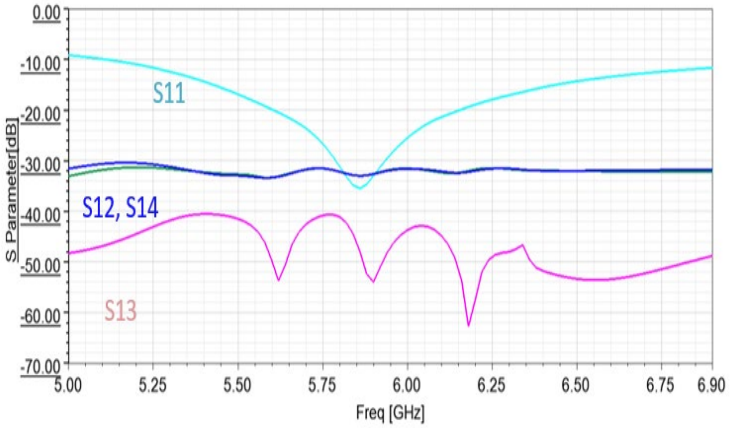

Figure 18: The simulated S parameters of the array at the center of a 5 feet diameter ground plane.

Figure 19 shows the 3D realized gain patterns in the upper hemisphere in both cartitian and polar format. In the polar plot, the zenith is at the center of the plot and the radial axis corresponds to elevation angle. These results confirm the desired radiation pattern characteristics as discussed in Figure 2 and Figure 3. It indicates that the antenna covers an azimuth range from -120 to 120 degrees and a vertical range from 0 to 90 degrees. This coverage aligns with our design requirements, ensuring that the antenna provides the desired directional radiation and gain. The 3D pattern further validates the effectiveness of the antenna in terms of its directional focus and radiation performance, making it suitable for the intended applications.

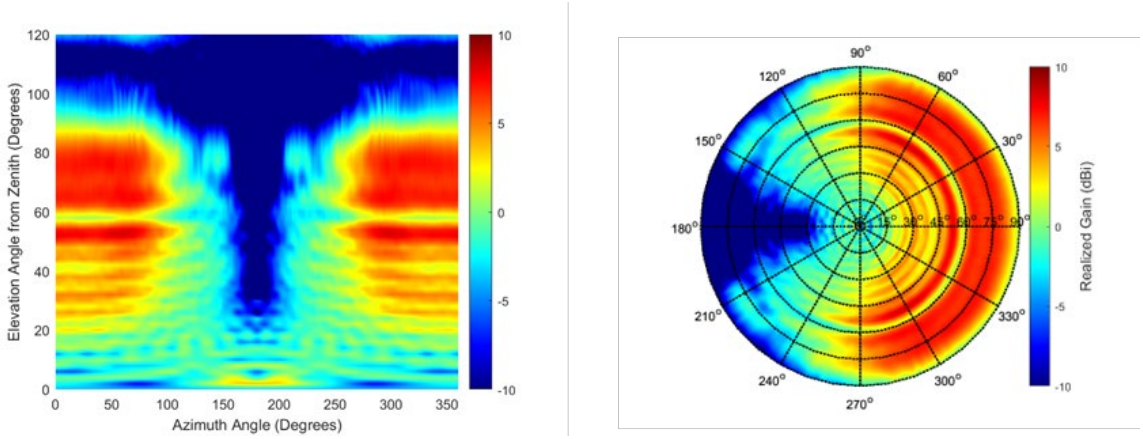

Figure 19: Simulated 3-D realized gain pattern of 5-ft GND case under single channel mode.

3.2.3 Impact of Ground Plane Sizes

From the azimuth radiation pattern in Figure 20, we observe that the gain of the antenna simulated on the infinite ground plane is higher than that of the antenna simulated on the 5 ft ground plane. This difference in gain can be attributed to the fact that the infinite ground plane provides ideal, uniform reflection and support for the antenna's radiation, maximizing its efficiency. In contrast, the finite 5 ft ground plane introduces edge effects, where diffraction and non-uniform reflections occur, leading to reduced gain. Additionally, the finite size of the ground plane limits the extent of the radiating surface, further contributing to lower overall gain.

In the vertical radiation pattern, we see that the antenna on the 5 ft ground plane exhibits more oscillations compared to the antenna on the infinite ground plane. This oscillation occurs because the edges of the 5 ft ground plane cause diffraction, resulting in out-of-phase fields that interfere with the antenna's main radiation. The finite plane introduces scattering at the boundaries, disrupting the smooth radiation pattern. Additionally, standing waves and reflections from the edges of the ground plane can contribute to the oscillatory behavior, distorting the pattern and affecting the stability of the antenna's radiation in the vertical plane.

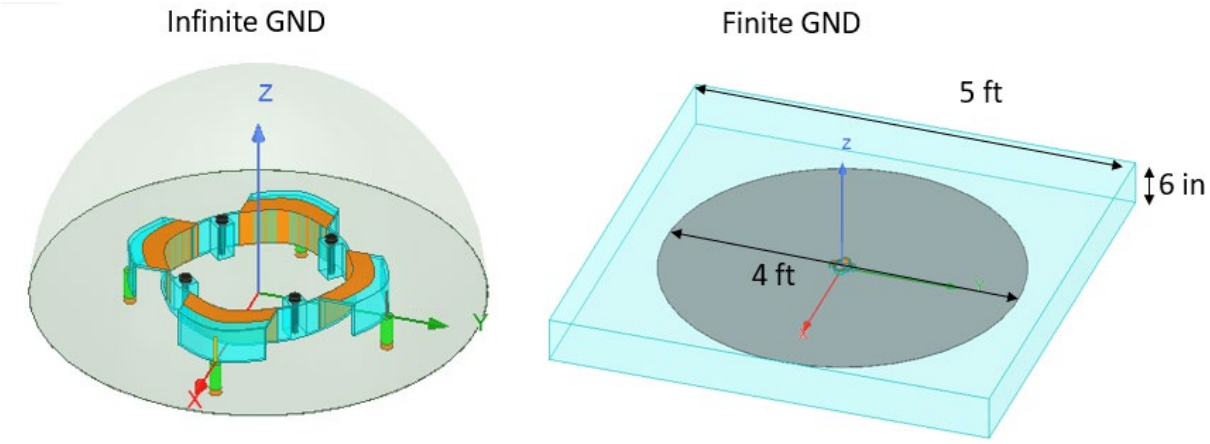

Figure 20: Configuration of Antennas in Infinte GND and Finite GND.

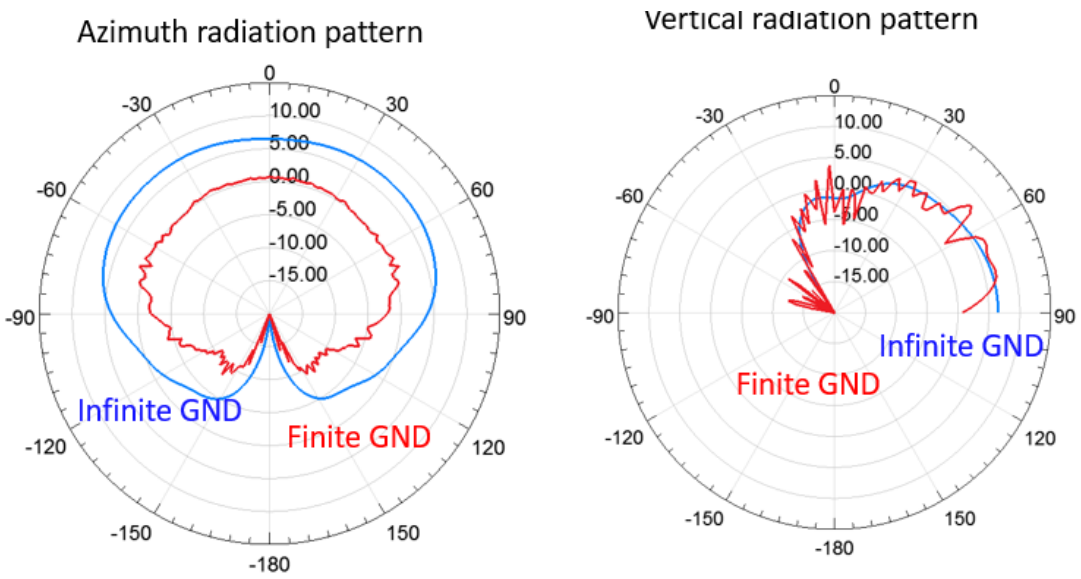

Figure 21: Radiation Patterns of Antennas on an infinite ground plane and a 5 feet ground plane.

4 Antenna Protype Fabrication

4.1 Antenna Parts and Assembling Process

The assembly process of the antenna involves several key components and steps. First, the four antenna strips and SMA connectors are attached to the sides of a 1mm thick ABS structure. This ABS material provides the necessary support and rigidity while maintaining minimal impact on the antenna's electrical performance due to its low dielectric loss. Next, we install four curved copper sheet reflectors around the antenna elements. These reflectors are strategically placed to enhance the antenna's radiation characteristics by directing the signals and improving overall gain.

Finally, the entire assembly is secured onto a 5 ft aluminum ground plane using four nylon screws. Nylon screws are chosen to prevent any unwanted interference with the antenna's performance, as they are non-conductive and ensure stable mounting without affecting the electromagnetic properties. This configuration ensures proper alignment and fixation of the antenna components, optimizing performance and maintaining structural stability during operation.

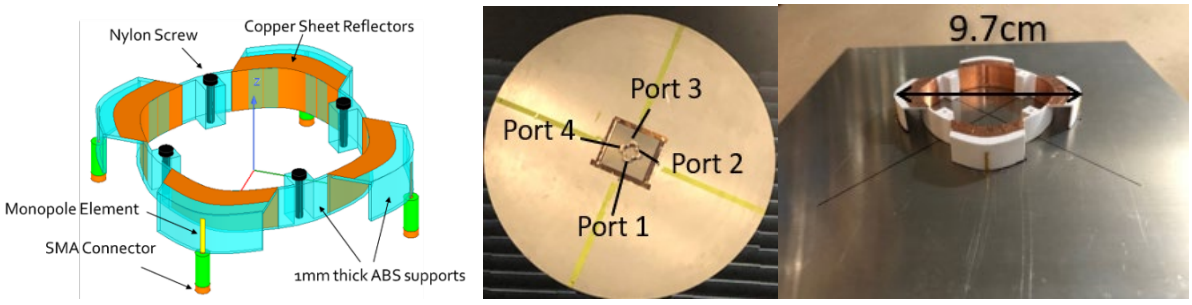

Figure 22: Antenna geometry and fabrication process.

5 Performance Validation Measurements

5.1 Measurement Setups

After assembling the antenna and mounting it on the 5 ft ground plane, the measurements were conducted in the anechoic chamber at the ElectroScience Lab, OSU, as shown in Figure 23. The setup involved placing the antenna on a positioner configured to rotate from -90 to 90 degrees along the azimuth axis (theta plane) and from 0 to 360 degrees in the elevation axis (phi plane), with a step size of 2 degrees for both axes to ensure detailed radiation pattern capture. During the measurement process, only one port was excited at a time, while the other ports were terminated with 50-ohm loads to prevent reflections and ensure accurate results. This method allows us to evaluate the performance of each antenna element individually, ensuring proper impedance matching and gain characteristics across the entire array.

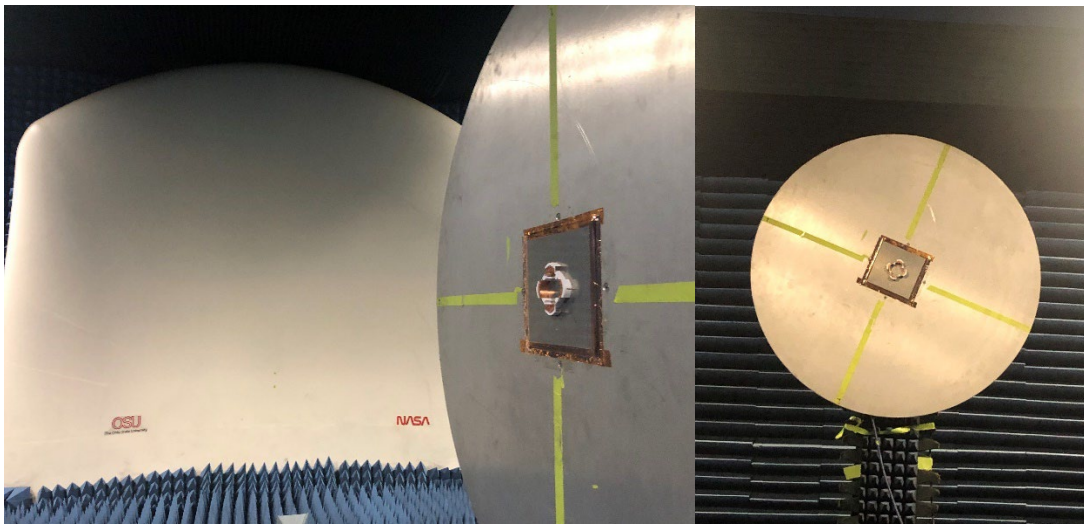

Figure 23: Measurement setup of antenna mounted on a 5 feet diameter ground plane.

5.2 Measurement Results

5.2.1 S Parameters

The comparisons of the S-parameters between the simulated and measured antenna are provided in Figure 24. It is evident that the measured data closely follow the same trend as the simulated data, indicating that the antenna's performance aligns well with the design expectations. However, we observe that the measured S13 data show more pronounced drops compared to the simulated S13 results. This discrepancy could be attributed to several factors. One possible reason is slight misalignments during the assembly process, which could affect the physical spacing and coupling between antenna elements. Additionally, measurement setup inaccuracies, might also contribute to the observed deviations in S13 performance. These factors combined could explain the differences between the simulated and measured mutual coupling behavior.

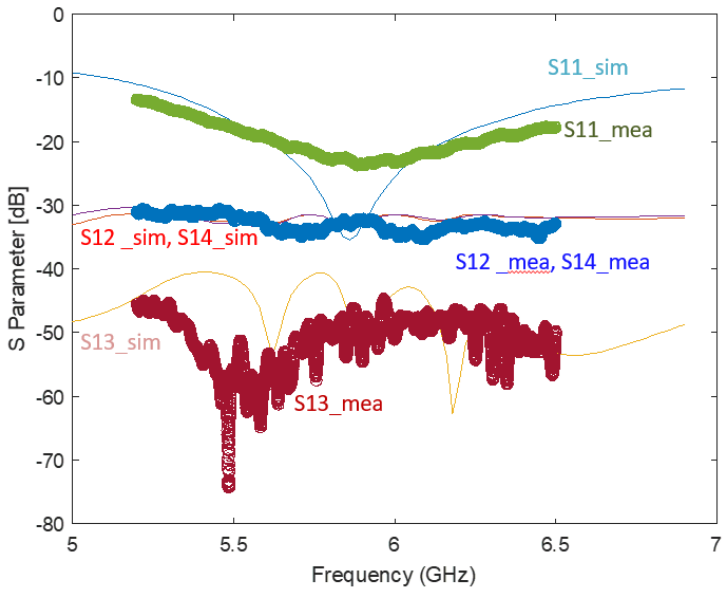

Figure 24: Measured S Parameters.

5.2.2 3-D Realized Gain Pattern

The comparisons of the 3D realized gain pattern between the simulated and measured antennas, shown in Figure 25 demonstrate a close match between the two data sets. The measured results closely follow the track of the simulated data, indicating that the antenna behaves as predicted. However, it can be observed that the simulated S13 data exhibits more oscillations than the measured S13 data. This discrepancy is due to the use of small gating during the measurement process, which helps filter out unwanted signals, such as reflections or noise, from the environment.

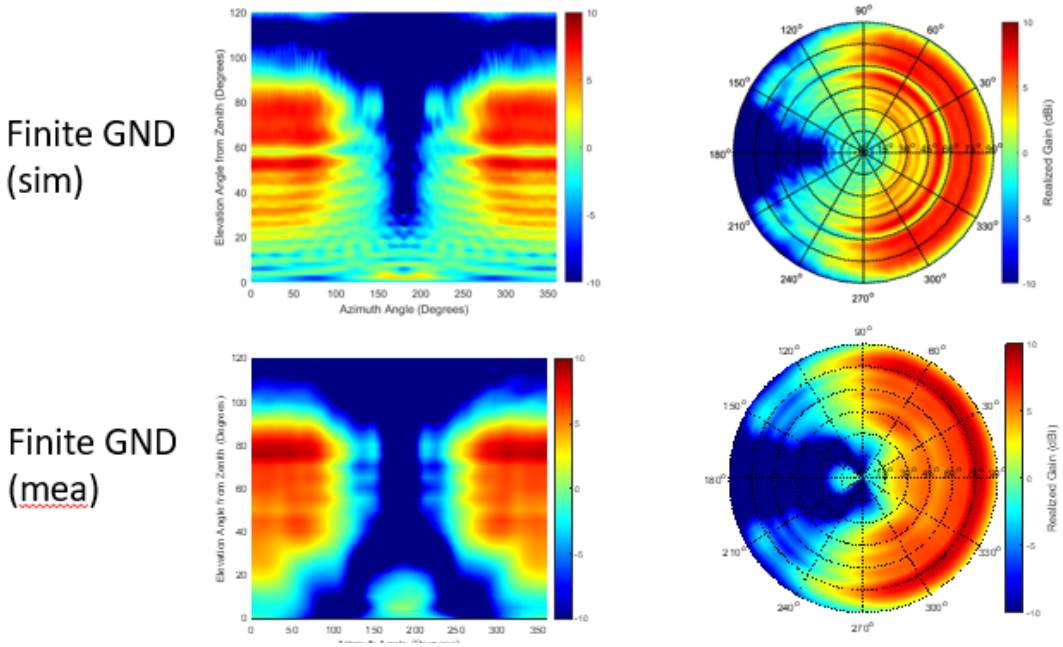

Figure 25: Measured and simulated 3-D realized gain pattern under single channel mode.

5.2.3 Maximum Selection MIMO Gain Pattern Coverage

Figure 26 illustrates the measured and simulated 3D realized gain patterns under the maximum selection mode. By analyzing this figure, we can derive the maximum gain at each angle, allowing us to compare the antenna's directional performance between the simulation and actual measurement. The measured gain closely aligns with the simulated data, indicating that the antenna performs as expected across various angles. Slight deviations may be present due to factors such as fabrication tolerances, environmental variations during testing, or minor imperfections in the measurement setup. Nonetheless, both patterns confirm that the antenna is optimized for maximum gain in its intended operational directions, validating the design's effectiveness in providing strong coverage and maintaining performance in the desired radiation zones. This alignment between simulated and measured results also demonstrates the reliability of the simulation model in predicting real-world antenna behavior.

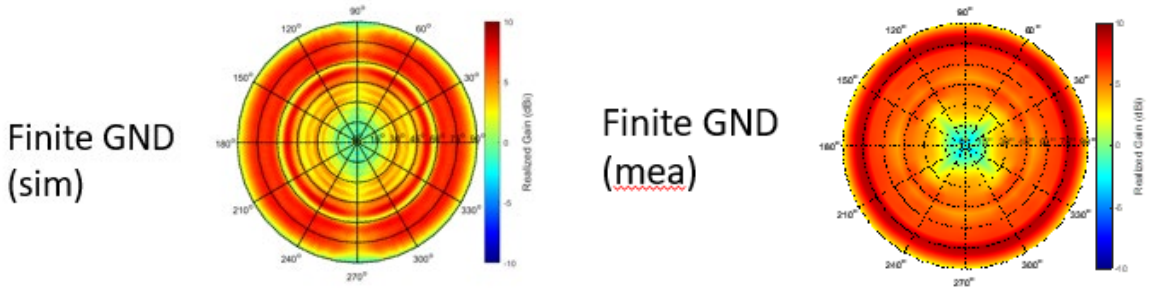

Figure 26: Measured and simulated 3-D realized gain pattern under maximum selection mode.

6 Reference

[1] Shah, G., Saifuddin, Md, Fallah, Y.P., Gupta, S.D.: RVE-CV2X: a scalable emulation framework for real-time evaluation of CV2X-based connected vehicle applications. In: 2020 IEEE vehicular networking conference (VNC) (2020).

[2] Nadeem Ahangar, M., Ahmed, Q.Z., Khan, F.A., Hafeez, M.: A survey of autonomous vehicles: enabling communication technologies and challenges. Sensors 21(3), 706 (2021).

[3] Position Navigation & Timing Technologies in the 21st Century, Wiley, January 2021. ISBN: 978-1-119-45849-4

[4] Lipfert, Hermann (August 2007). MIMO OFDM Space Time Coding – Spatial Multiplexing, Increasing Performance and Spectral Efficiency in Wireless Systems, Part I Technical Basis (Technical report). Institut für Rundfunktechnik.

[5] X. Mei and K. -L. Wu, "Envelope Correlation Coefficient for Multiple MIMO Antennas of Mobile Terminals," 2020 IEEE International Symposium on Antennas and Propagation and North American Radio Science Meeting, Montreal, QC, Canada, 2020, pp. 1597-1598, doi: 10.1109/IEEECONF35879.2020.9329678.